Iterative joint inversion of P-wave and S-wave crosswell traveltime data

Tieyuan Zhu and Jerry M. Harris, Department of Geophysics, Stanford University*

SUMMARY

Joint inversion of multiple geophysical data-sets is promising to reduce uncertainties in independently inverted models. Here, we present an iterative joint inversion approach for P and S traveltime data using cross-gradient function as constraint term. This type of joint inversion scheme links independent inversions through iterations and the cross-gradient function. The primary advantage of this joint inversion strategy is to avoid determining relative weighting of different data-sets. To investigate the performance of this method, we test our algorithm in synthetic examples of P and S traveltime data and field data acquired in west Texas. The results of synthetic example show that the joint inversion significantly reduces the ambiguities of inverted models and improves the identification of boundaries. In results of field data, jointly inverted S velocities have better correlation with P velocities. Moreover, lithologies delineated from Vp/Vs map by joint inversion matches log data very well and also shows clearly a dipping structure below reservoir that was not shown in previous crosswell tomography results.

INTRODUCTION

Joint inversion approaches are considered to be a promising strategy to reduce ambiguities in independent models (e.g. Haber and Oldenburg, 1997; Gallardo and Meju, 2003; Colombo and De Stefano, 2007; Hu et al., 2009). Basically, joint inversion refers to combining several geophysical data-sets in a single inversion algorithm and then simultaneously solving least squares problem (Vozoff and Jupp, 1975). The resultant models satisfy all collected data simultaneously. Hence the null space for one data-set may be resolved by another data-set (Julia et al., 2000). The explanation is that different measurements tend to have different resolving kernels and then may complement each other.

Although a simultaneous joint inversion provides acceptable solutions, it still faces some difficulties that affect its performance: firstly, it requires more memory as the huge coupled jacobian and/or hessian matrix for different inversions have to be computed and/or saved at the same time (Hu et al., 2009); second, the determination of suitable relative weighting between different objective functions could be challenging; In reality, a correct and effective link between two models in joint inversion could reduce the uncertainties, but petrophysical relationships and geological structure, may not be improved when we blindly invert two or more data-sets with widely different resolutions in a single inversion.

Instead of a simultaneous joint inversion, in this paper, we formulate an iterative joint inversion approach for the cross-well tomography problem that is quite similar to the ones of Hu et al. (2009) and Heincke et al. (2010). This iterative joint inversion couples independent inversions through iteration with a cross-gradient function. At every iteration, the updated model are used as constraints for the next models. This approach overcomes the memory issue and the determination of relative weighting of different data sets. Moreover, The potential advantage for this algorithm is to incorporate prior models easily in the inversion algorithm. For example, a prior lithologic map (e.g from reflection images or welllogs) could be applied as other parameters in the cross-gradient function.

One concern of this joint inversion approach is to converge to local minimum. We have to adjust the strengths of the cross-gradient constraints at each step to avoid that the convergence of the inversions is over disturbed by this constraint term. Therefore, the resultant models tend to converge in terms of data itself.

Finally, we apply this algorithm on a simple synthetic test problem and on a crosswell seismic monitoring reservoir data set acquired at the West Texas sequestration site.

METHODOLOGY

The inverse problem is formulated as an optimization that involves minimization of an objective function Φ, that combines a measure of data misfit Φ_d, and a regularization measure Φ_m, with the constraint function between different models Ψ:

$$\min \Phi(\mathbf{m}) = \Phi_d(\mathbf{m}) + \lambda \Phi_m(\mathbf{m}) + \beta \Psi(\mathbf{m}) \qquad (1)$$

Here $\mathbf{m}$ is the model vector that is the spatial function m(x,y,z) and λ and β are the regularization coefficients, which are used to adjust contributions for data misfit from the model regularization term and the constrain function.

For our problem, the cross gradient function is chosen as the constraint functional Ψ. The objective function of

joint inversion of two data sets are defined as

$$\Phi(\mathbf{m}_1) = \Phi_d(\mathbf{m}_1) + \lambda_1\Phi_m(\mathbf{m}_1) + \beta_P\Psi_{cg}(\mathbf{m}_1,\mathbf{m}_2),$$
$$\Phi(\mathbf{m}_2) = \Phi_d(\mathbf{m}_1) + \lambda_2\Phi_m(\mathbf{m}_2) + \beta_S\Psi_{cg}(\mathbf{m}_1,\mathbf{m}_2). \quad (2)$$

where the first term is data misfit

$$\Phi_d(\mathbf{m}_i) = \|W_d(G(\mathbf{m}_i) - \mathbf{d_{obs}}^i)\|_2^2, i = 1,2. \quad (3)$$

$G(\mathbf{m})$ is the forward functional. $\mathbf{d_{obs}}$ is the observed data vector while $\mathbf{m}$ is the unknown model vector. $\mathbf{W_d}$ is the data weighing matrix. The regularization terms Φ_m are chosen by the first-order derivative in spatial directions (Li and Oldenburg, 2000). The constraint functional is $\Psi_{cg}(\mathbf{m}_1,\mathbf{m}_2) = \|t\|_2^2$. The cross-gradient function t is defined as (Gallardo and Meju, 2003):

$$t(x,y,z) = \vec{\nabla}m_1(x,y,z) \times \vec{\nabla}m_2(x,y,z), \quad (4)$$

$\vec{\nabla}$ is gradient in x, y and z directions. The jacobian of the cross-gradient with respect to model parameters is given in (Gallardo, 2004).

The regularization coefficient λ is crucial for stabilizing inversion and obtaining suitable solutions. In our synthetic example, we carefully choose λ through several tests to balance model misfit and data misfit. For field data, λ is selected manually by several trial runs. When λ is obtained, we hold this fixed value during all iterations. The coefficient β controls the influence from other models on the solution. A large value of β usually is chosen to force the cross-gradient functional term to minimum so that unknown models will be more similar. It is determined by the experience rule given by Hu et al. (2009): $|\Phi_d(\mathbf{m}_k)|^2/(|\Psi_{cg}(\mathbf{m}_k)|^2 + \delta^2)\frac{10^L}{N_xN_yN_z}$, where δ is a small value. L is a trial-and-error number that depends on which model is superior, i.e., the superior model has relatively small weights. N_x, N_y and N_z are the number of discretized grids in the x, y and z direction.

A flowchart of our iterative procedure is shown in Figure 1. The procedure begins with two input data-sets and corresponding initial models $m_0 = (m_1, m_2)$ that are the best known representations of the subsurface. Then, the joint term J is computed and then the following step is to minimize the objective function (Equation 2) in A and B respectively to obtain new models m_1 and m_2. The procedure is repeated iteratively until the stop criteria are satisfied. The output inversion results are the optimal solutions $m_{optimal} = (m_1, m_2)$.

Traveltimes in the forward modeling are computed by solving the Eikonal equation using the finite-difference method and the raypaths from a receiver to the source

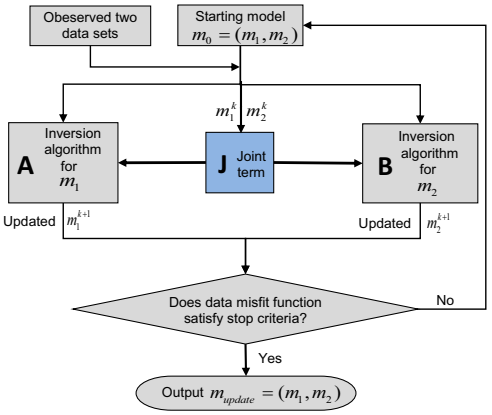

Figure 1: Flowchart of iterative joint inversion.

are determined by back propagation (Zelt and Barton, 1998). We use a Gauss-Newton strategy to solve the above inverse scheme.

SYNTHETIC EXAMPLE

To demonstrate the applicability of our iterative joint inversion algorithm, we test it on a typical reservoir model (Ensley, 1984) in crosswell geometry. The true model is a layered structure with a reservoir embedded in the second layer, as shown in Figure 2a. This model is difficult for either the P-wave or S-wave method alone to resolve. We will see whether joint inversion of P and S data will help resolve the ambiguities. Synthetic traveltimes data were generated from the true model in Figure 2 by the Eikonal solver (Vidale, 1990). The starting models for P- and S-wave are homogeneous with mean values of the true models. A total of ten iterations were performed which was proven to make the Gauss-Newton method to converge.

Independent inversions

In this example, no noise is added. The regularization parameters λ are 2×10^{-5} and 3×10^{-5} for P- and S-wave model inversion algorithm, respectively. Independent inversion results of P- and S-wave velocities, and the cross gradient values of two velocities are shown in Figure 2d-f. The inverted P-wave model is quite good, especially about the gas-water contact, because the velocity contrast between gas and water is very high. However, the geometry of the objects are not well recovered because of ray coverage and the smoothing property of regularization term. For the inverted S-wave velocity model in Figure 2e, the geometry of gas-water body is better defined since relatively high velocity gas-water body have better ray coverage, but the lack of resolution about contact is observed. The central-right panel

(f) shows the structural similarity of inverted P-wave velocity (d) and S-wave velocity model (e).

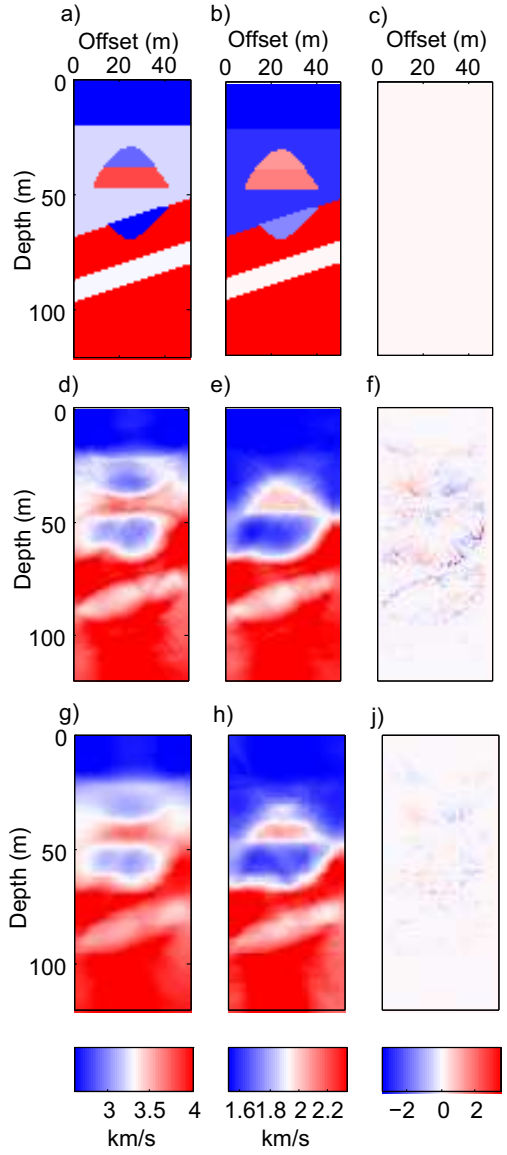

Figure 2: Two-dimensional crosswell seismic test model and inverted models. a-c: true P-wave, S-wave velocity model and cross-gradient map between two models; d-f: Corresponding results by independent inversion; g-j: Corresponding results by joint inversion. The same scale colorbar is labeled in bottom.

Joint inversion

Next, we invert the P and S-wave synthetic data using the iterative joint inversion algorithm. We use the same regularization λ that we used with the independent inversions above. Figure 2g-j shows the joint inversion results. Notably, the edge of the reservoir in the P-wave velocity model is improved. Furthermore, the gas-water

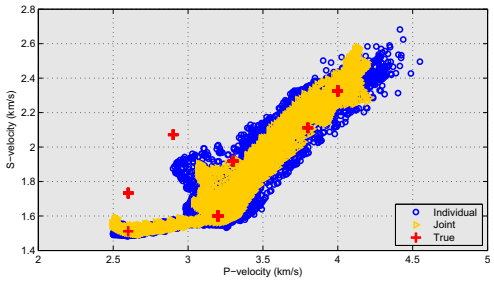

Figure 3: Crossplot of P- and S-wave velocity models

contact is better resolved in the inverted S-wave velocity model. On whole, the joint inversion results tend to remove artifacts shown in independent inversion results. To evaluate the performance of the cross-gradient similarity constraint of the joint-inversion algorithm, we plot the cross-gradient value for the independent (Fig. 2f) and joint inversion (Fig. 2j). It is obvious that cross-gradient values by joint inversion are closer to zero as designed. The root mean square (RMS) value ($\sqrt{\|t\|^2/N_xN_z} * 1e6$) at the final step decreases to (~ 0.09) from (~ 0.25) of independent inversion results. It says that the structure of resultant models with cross-gradient constraint are more similar as we expected.

We plotted the P- and S-wave velocity cross-plots from all recovered models in Fig. 3. Seven true value (Red cross) represent seven different blocks in synthetic models (Fig. 2a-b). The independent inversion values are plotted by the blue circles while the joint inversion ones are by the yellow stars. It is pronounced that these P-S velocity values of the joint inversion models are less dispersed than those obtained from the separate inversion results.

FIELD EXAMPLE

We now consider seismic P and S traveltime data collected between wells in a west Texas for reservoir delineation and CO2 monitoring project. We choose the baseline data recorded in 1993 before CO2 injection since it has a relative good quality S wave picks for my purpose. The original P and S-wave traveltime data are seen in Fig.6 in Harris et al. (1995). The picks with angle less than 45° degree are selected for inversion. From the previous study, we know the lithology is quite flat so we put 10 times horizontal regularization than vertical. The regularization parameter λ for P- and S-wave models are kept consistent during independent and joint inversion procedure.

Figure 4 show the results of inversions for P and S-

velocity models as well as the ratio of two velocities. The models by joint inversion (Fig. 4e-h) correlate better. The layer around depth 2.6kft and 2.7kft is more pronounced in the S-velocities. The resultant Vp/Vs ratio map has few artifacts and appears more reasonable for use in geological interpretation than the independent inversions. We further evaluated the inversion results by looking at the spatial distribution of cross-gradient values. The extreme large values appears in the result by independent inversions (Fig. 4d) while joint inversion result (Fig. 4h) is highly averaged. The corresponding RMS values are 310.0 (Independent) and 280.0 (Joint), respectively. The data misfit between the measured data and the predicted data is comparable between independent and joint inversion in Table 1.

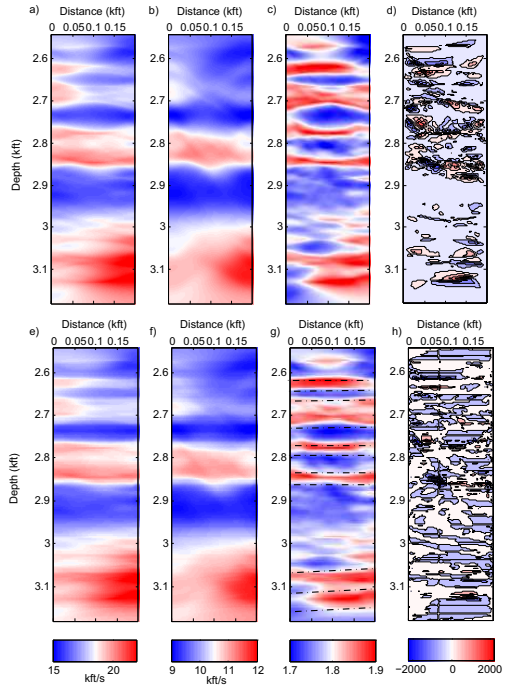

Figure 4: Inverted models by independent (a-d) and joint inversions(e-h). a-d: Inverted P-wave, S-wave velocity model, Vp/Vs and cross-gradient values between two models by independent inversion; e-h: Corresponding results by joint inversion.

Table 1: RMS values

	Independent	Joint
RMS of P data misfit	0.0431	0.0455
RMS of S data misfit	0.0865	0.0889
RMS of cross gradient	310.0	280.0

From figure 5, the lithological Vp/Vs model shows good agreement with porosity log data. In particular, the dipping ($\sim 8^{\circ}$) interface below 3.05kft is observed, which is ambiguous in independent inversions. Therefore, the iterative joint inversion approach leads to better results in this field data case.

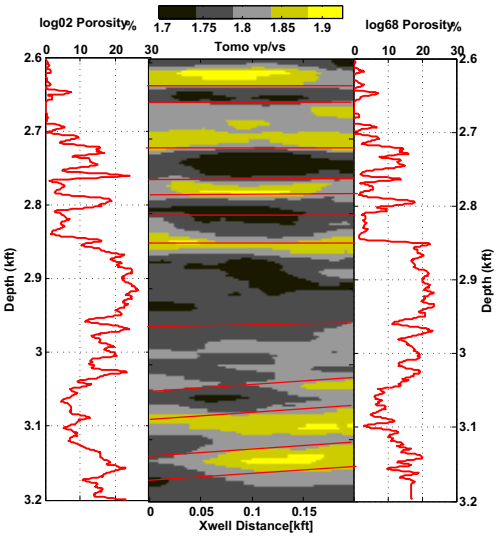

Figure 5: Jointly inverted Vp/Vs with porosity log data.

DISCUSSION AND CONCLUSION

An iterative joint inversion approach is presented. It is different from the simultaneous joint inversion for coupling independent inversions in every iteration with constraint function (e.g. cross-gradient function). For simultaneous joint inversion, carefully taken regularization coefficients and relative weights between multiple models are needed to for convergence for a predefined data error. A more sophisticated line search method requires more computations (Linde et al., 2008). Our iterative joint inversion strategy avoids this selection of relative weights and thus reduce computational costs. Examples from synthetic and field P and S picks data are used to demonstrate feasibility.

We intend to continue research on different characteristic data (like seismic and gravity data). Further work are needed to evaluate the performance of this joint inversion before its conclusion.

ACKNOWLEDGEMENT

The author would like to thank Youli Quan for many discussions.

EDITED REFERENCES

Note: This reference list is a copy-edited version of the reference list submitted by the author. Reference lists for the 2011 SEG Technical Program Expanded Abstracts have been copy edited so that references provided with the online metadata for each paper will achieve a high degree of linking to cited sources that appear on the Web.

REFERENCES

Colombo, D., and M. De Stefano, 2007, Geophysical modeling via simultaneous joint inversion of seismic, gravity, and electromagnetic data: Application to prestack depth imaging: The Leading Edge, **26**, 326–331, doi:10.1190/1.2715057.

Ensley, R. A., 1984, Comparison of P- and S-wave seismic data: A new method for detecting gas reservoirs: Geophysics, **49**, 1420–1431.

Gallardo, L. A., 2004, Joint two-dimensional DC resistivity and seismic travel time inversion with cross-gradients constraints: Journal of Geophysical Research, **109**, B3, 1–11, doi:10.1029/2003JB002716.

Gallardo, L. A., and M. A. Meju, 2003, Characterization of heterogeneous near-surface materials by joint 2D inversion of DC resistivity and seismic data: Geophysical Research Letters, **30**, no. 13, 1658–1661, doi:10.1029/2003GL017370.

Haber, E., and D. Oldenburg, 1997, Joint inversion: a structural approach: Inverse Problems, **13**, no. 1, 63–77, doi:10.1088/0266-5611/13/1/006.

Harris, J. M., R. C. Nolen-Hoeksema, R. T. Langan, M. V. Schaack, S. K. Lazaratos, and J. W. Rector, 1995, High-resolution crosswell imaging of a west Texas carbonate reservoir: Part 1 — Project summary and interpretation: Geophysics, **60**, 667–681, doi:10.1190/1.1443806.

Heincke, B., M. Jegen, M. Moorkamp, J. Chen, and R. W. Hobbs, 2010, Adaptive coupling strategy for simultaneous joint inversions that use petrophysical information as constraints: 80th Annual International Meeting, SEG, Expanded Abstracts, **29**, 2805–2809.

Hu, W., A. Abubakar, and T. M. Habashy, 2009, Joint electromagnetic and seismic inversion using structural constraints: Geophysics, 74, no. 6, R99–R109.

Julià, J., C. J. Ammon, R. B. Herrmann, and A. M. Correig, 2000, Joint inversion of receiver function and surface wave dispersion observations: Geophysical Journal International, **143**, no. 1, 99–112, doi:10.1046/j.1365-246x.2000.00217.x.

Li, Y., and D. W. Oldenburg, 2000, Incorporating geological dip information into geophysical inversions: Geophysics, **65**, 148–157, doi:10.1190/1.1444705.

Vidale, J. E., 1990, Finite-difference calculation of traveltimes in three dimensions: Geophysics, **55**, 521–526, doi:10.1190/1.1442863.

Vozoff, K., and D. L. B. Jupp, 1975, Joint inversion of geophysical data: Geophysical Journal of the Royal Astronomical Society, **42**, no. 3, 977–991, doi:10.1111/j.1365-246X.1975.tb06462.x.

Zelt, C., and A. Barton, 1998, Three-dimensional seismic refraction tomography: A comparison of two methods applied to data from the Faroe basin: Journal of Geophysical Research, **103**, B4, 7187–7210, doi:10.1029/97JB03536.